nature nanotechnology

ARTICLES

PUBLISHED ONLINE: 26 MAY 2013 | DOI: 10.1038/NNANO.2013.92

Two DNA nanomachines map pH changes along intersecting endocytic pathways inside the same cell

Souvik Modi[1], Clément Nizak[2], Sunaina Surana[1], Saheli Halder[1] and Yamuna Krishnan[1]*

DNA is a versatile scaffold for molecular sensing in living cells, and various cellular applications of DNA nanodevices have been demonstrated. However, the simultaneous use of different DNA nanodevices within the same living cell remains a challenge. Here, we show that two distinct DNA nanomachines can be used simultaneously to map pH gradients along two different but intersecting cellular entry pathways. The two nanomachines, which are molecularly programmed to enter cells via different pathways, can map pH changes within well-defined subcellular environments along both pathways inside the same cell. We applied these nanomachines to probe the pH of early endosomes and the trans-Golgi network, in real time. When delivered either sequentially or simultaneously, both nanomachines localized into and independently captured the pH of the organelles for which they were designed. The successful functioning of DNA nanodevices within living systems has important implications for sensing and therapies in a diverse range of contexts.

DNA has been molecularly chiselled to create a variety of intricate architectures on the nanoscale[1]. DNA nanoarchitectures that can be triggered chemically or physically to switch between defined states (referred to as DNA nanomachines) have great potential for robotic and sensing applications on the nanoscale[2,3], and subcellular compartments provide nanoscale environments that offer rich possibilities for demonstrating the functionality of these nanoarchitectures[4]. It was recently demonstrated that a DNA nanomachine can function as a pH sensor inside endosomes *in cellulo*[5] as well as *in vivo*[6]. Since then, a few exciting applications of specific DNA nanostructures have been demonstrated *in cellulo*[6–9]. However, achieving simultaneous functionality of multiple DNA nanomachines within the same cell remains a challenge, which, if realized, would open up possibilities of multiplexing DNA nanodevices in living systems. The precise positioning of more than one DNA nanodevice within a subcellular environment and demonstration of their simultaneous functionality therein is therefore essential. Here, we apply the technology we term 'SimpHony' (simultaneous pH mapping technology) to deploy two differently programmed DNA nanomachines along different cellular endocytic pathways and map pH changes along both pathways simultaneously, within the same living cell.

Programming strategy to achieve SimpHony

Simultaneous mapping of an analyte such as pH using fluorescence resonance energy transfer (FRET)-based DNA nanomachines requires molecular programming strategies that position each nanomachine along a distinct pathway, as well as a combination of FRET pairs with minimal crosstalk. SimpHony also requires two pH-responsive DNA nanomachines with pH-sensitive regimes suited to the lumenal pH of the relevant intracellular organelles being investigated. We chose two well-characterized pathways: the furin retrograde endocytic pathway and the transferrin endocytic/recycling pathway. Furin resides predominantly in the trans-Golgi network (TGN), with a small steady-state population at the plasma membrane, and is transported retrogradely via the early endosomes/sorting endosomes (EE/SEs) and late endosomes (LEs) to the TGN in a Rab-9-dependent manner[10,11]. Transferrin binds the transferrin receptor at the plasma membrane, reaches the EE/SEs and then the perinuclear recycling endosome (RE)[12]. The transferrin and furin pathways merge in the EE and then segregate thereafter into the RE and LE, respectively.

To track the furin pathway, we used a molecularly programmed DNA nanomachine called I^{Fu} (Fig. 1a). This adopts the same working principle as described previously[5,6] and is programmed such that (i) the position of the acceptor is optimized to maximize the observed FRET, (ii) the FRET pair uses Alexa 546 as a donor fluorophore, which allows compatibility of I^{Fu} pH measurements in the presence of I^{Tf} fluorophores, and (iii) I^{Fu} incorporates an 8 bp dsDNA sequence (shaded in grey in Fig. 1a) that functions as a binding site for an engineered protein (grey cylinders) that enables its localization to a given endocytic pathway, namely the furin pathway. Because furin is a retrogradely transported membrane protein that lacks a natural ligand, we developed a method to specifically attach and transport a DNA nanostructure to such a trafficking protein. This uses a sequence-specific double-stranded DNA (dsDNA) binding protein (single-chain variable fragment recombinant antibody, or scFv)[13], which is expressed as a chimera with furin. This sequence-specific, dsDNA-binding protein was obtained from a phage display screen of scFv recombinant antibodies against a dsDNA epitope. This scFv specifically binds a dsDNA sequence $d(AT)_4$ (Fig. 1c) with a dissociation constant K_D of ~80 nM (Fig. 1d). Thus an *N*-terminal fusion of the scFv domain with furin, when expressed inside cells, will act as an artificial receptor for a DNA nanostructure that incorporates a $d(AT)_4$ sequence and will traffic the latter along the retrograde furin endocytic pathway into the TGN (Fig. 1b).

To track the transferrin pathway, we engineered a two-stranded pH-sensitive DNA nanomachine, I^{Tf} (Fig. 1a). I^{Tf} uses intrastrand i-motif formation to undergo a pH-dependent conformational change and therefore functions as a FRET-based pH sensor. I^{Tf} has a pH-responsive C-rich segment, shown in purple in

[1]National Centre for Biological Sciences, TIFR, GKVK, Bellary Road, Bangalore 560065, India, [2]Laboratoire Interdisciplinaire de Physique, UMR5588 CNRS-Université Grenoble I, Grenoble, France. *e-mail: yamuna@ncbs.res.in

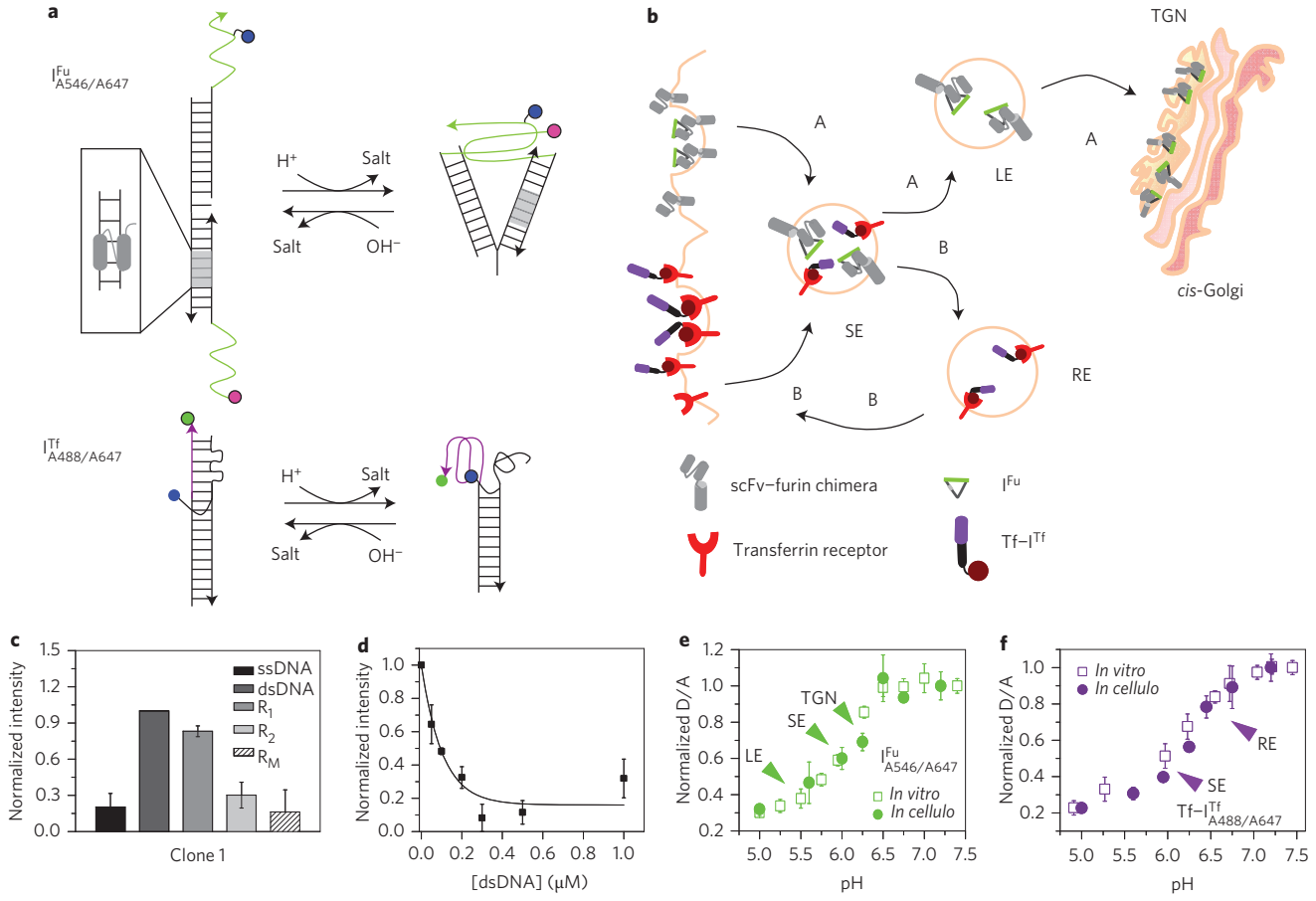

Figure 1 | Programming of DNA nanodevices. a, Schematic of the DNA nanomachines that map the furin (Fu) and transferrin (Tf) pathways: I^{Fu} (top) and I^{Tf} (bottom). I^{Fu} consists of a nicked duplex and cytosine-rich overhangs and undergoes a pH-dependent conformational change due to i-motif formation (green segment), leading to high FRET between Alexa 546 (magenta circle) and Alexa 647 (blue circle) labels on the scaffold. A dsDNA domain on I^{Fu} (grey) acts as a recognition element for a recombinant antibody (scFv, grey cylinders) that confines I^{Fu} along the Fu pathway. I^{Tf} is a duplex containing a pH-responsive element (purple strand) and forms an intramolecular i-motif at low pH, leading to high FRET between Alexa 488 (green circle) and Alexa 647 (blue circle) labels on the scaffold. Coupling transferrin (Tf) to I^{Tf} confines Tf-I^{Tf} to the Tf receptor pathway. **b**, Schematic of SimpHony. An scFv–furin chimera (grey) retrogradely transports I^{Fu} into the TGN (pathway A) via the SE and LE. Tf-I^{Tf} marks the SE en route to the RE (pathway B). **c**, dsDNA sequence-specific binding capacity of the scFv (clone C1) illustrated using different DNA epitopes. See Supplementary Table S1 for sequences of the epitopes ssDNA, dsDNA, R_1, R_2 and R_M. Error bars indicate ±s.d. **d**, scFv binding to immobilized dsDNA in the presence of increasing competitor dsDNA. Error bars indicate ±s.e.m. **e**,**f**, Donor (D) to acceptor (A) ratio measurements on dually labelled DNA nanomachines I^{Tf} and I^{Fu} *in vitro* and *in cellulo* as a function of pH. Ratio of intensities at 570 nm (D) and 669 nm (A) for $I^{Fu}_{A546/A647}$ (**e**) and at 520 nm (D) and 669 nm (A) for $I^{Tf}_{A488/A647}$ (**f**) when excited at 546 nm and 488 nm, respectively, under pH-clamped conditions. Experiments were performed in triplicate and expressed as mean±s.d. Arrowheads indicate the typical reported pH in the literature of the indicated subcellular compartments.

Fig. 1a, which partially base-pairs with a G-rich overhang in the complementary strand to form a weak duplex. At low pH, this duplex frays, allowing the C-rich strand to fold into an intramolecular i-motif. By chemically conjugating transferrin (Tf) to one of the strands in I^{Tf} to give Tf–I^{Tf}, one can molecularly program I^{Tf} to be confined along the transferrin receptor pathway (Fig. 1b).

Different cellular organelles have different lumenal pH values—ranging from pH 4.8 (lysosome) to pH 7.1 (endoplasmic reticulum)—so it is important to have DNA nanomachines with a suitable pH response for the relevant organelle as well as appropriate FRET pairs for simultaneous measurements[14–16]. The performances and working pH regimes of the DNA nanomachines engineered for the furin and transferrin pathways, respectively, are shown in Fig. 1e,f. From the many fluorophore pairs tried, we found the best FRET pairs to be Alexa 488/Alexa 647 (A488/A647) and Alexa 546/Alexa 647 (A546/A647), which demonstrated maximal FRET and minimal crosstalk when used simultaneously. Thus, I^{Tf} carried A488/A647 as its FRET pair ($I^{Tf}_{A488/A647}$) and I^{Fu} carried A546/A647 as its FRET pair ($I^{Fu}_{A546/A647}$) (Supplementary Fig. S1). $I^{Fu}_{A546/A647}$ showed a pH sensitivity from pH 5 to 6.5, suitable for studying pH variations in the EE/SEs, LEs and TGN, with typical intraorganelle pH values as indicated by the green arrowheads in Fig. 1e. $I^{Tf}_{A488/A647}$ showed a transition from pH 5.5 to pH 7, spanning the EE/SE and RE pH values, with typical intraorganelle pH values indicated by the purple arrowheads in Fig. 1f.

Each DNA nanomachine maps pH of its targeted pathway

When the scFv–furin chimera was expressed inside HeLa cells, two closely spaced bands near the expected size (43–45 kDa) (Supplementary Fig. S2) indicated that the fusion protein mimics the maturation of endogenous furin (Supplementary Fig. S3a–c)[17], and it is also localized, like endogenous furin, to the TGN (Supplementary Fig. S3d)[18]. When scFv–furin-expressing HeLa and TRVb-1 cells were incubated with 500 nM $I^{Fu}_{A488/A647}$ in the external medium and imaged, we observed that $I^{Fu}_{A488/A647}$ was efficiently endocytosed into perinuclear compartments; this did not occur in untransfected or mock transfected cells

(Supplementary Fig. S4a–d). A competitive endocytic uptake assay revealed that the *N*-terminal scFv domain of the scFv–furin acts as a highly specific, artificial receptor for a DNA scaffold containing the 8 bp $d(AT)_4$ tag, efficiently internalizing any DNA device incorporating this sequence (Supplementary Fig. S4).

Co-localization experiments, performed with molecular markers for SEs, LEs and TGN in IA2.2 cells expressing scFv–furin, demonstrated that I^{Fu} marks the furin retrograde pathway (Fig. 2; Supplementary Figs S2,S3). When these cells were labelled with a 10 min pulse of a cocktail of Alexa 568-labelled transferrin (Tfn_{A568}) and $I^{Fu}_{A488/A647}$ and imaged, they showed significant co-localization, indicating that, post-endocytosis, I^{Fu} is predominantly resident in the EE/SEs (Fig. 2a,f). When cells were labelled for 1 h with a cocktail of $I^{Fu}_{A546/A647}$ and fluorescein isothiocyanate (FITC)–dextran, and chased for 1 h, they showed significant co-localization (Fig. 2b,g) revealing that I^{Fu} had trafficked from the EE/SEs into the LEs. Upon labelling cells with $I^{Fu}_{A546/A647}$ for 2 h in the presence of 125 μg ml^{-1} cycloheximide and chasing for 90 min, we observed that I^{Fu} was trafficked onwards from the LEs (Supplementary Fig. S4b,c,e), accumulating in a perinuclear compartment distinct from the lysosome and Golgi (Supplementary Fig. S5a,b). This $I^{Fu}_{A546/A647}$-containing compartment was confirmed to be the TGN by co-localization experiments with NBD-C6-ceramide and anti-TGN46 antibodies (Fig. 2c,h, Supplementary Fig. S5c). Thus, the scFv domain on scFv–furin functions as an artificial receptor for DNA nanostructures bearing a $d(AT)_4$ dsDNA tag and is stable inside cells for up to 3 h (Supplementary Fig. S6).

The transferrin receptor pathway was next marked using I^{Tf} conjugated to human holo-transferrin using *N*-succinimidyl-3-(2-pyridyldithio)propionate to give $Tf\text{–}I^{Tf}_{A488/A647}$ (Supplementary Figs S7–S9). When a cocktail of Tfn_{A568} and $Tf\text{–}I^{Tf}_{A488/A647}$ was used to pulse the cells for 10 min, they co-localized in the SEs (Fig. 2d,i). When Tfn_{A568} and $Tf\text{–}I^{Tf}_{A488/A647}$ were pulsed for 10 min and chased for 12 min, they co-localized in the perinuclear REs (Fig. 2e,j). Thus, DNA nanostructures programmed to display endocytic ligands may be trafficked down the specific endocytic pathway of their corresponding receptor without perturbing the trafficking characteristics of the ligand.

The intracellular performances of $Tf\text{–}I^{Tf}_{A488/A647}$ and $I^{Fu}_{A546/A647}$ were assessed individually by their endocytosis into scFv–furin-expressing IA2.2 cells. Post-endocytosis, the intracellular pH was clamped at values between pH 5 and 7.5 and the donor to acceptor (D/A) ratios plotted as a function of pH, as described[5,6]. These showed that the *in vitro* pH response characteristics of both DNA nanomachines were preserved *in cellulo* (Fig. 1e,f). Spatiotemporal pH mapping was then performed separately with each nanomachine. EE/SEs were labelled with $I^{Fu}_{A546/A647}$ as described, and a histogram of the pH values for all such labelled SEs revealed a pH distribution with a mean pH of 5.98 ± 0.02, in line with the literature (Fig. 3a–c)[19]. Interestingly, when the LEs of scFv–furin-expressing cells were labelled with $I^{Fu}_{A546/A647}$, as described, the pH distribution of endosomes revealed a distinct shift to lower D/A values, corresponding to a pH of 5.72 ± 0.08, consistent with the literature (Fig. 3d–f)[20]. When the TGN of these cells was labelled with $I^{Fu}_{A546/A647}$ as described, the degree of spatial pH heterogeneity was found to be 6.18 ± 0.01 (Fig. 3g–i)[21]. Similarly, the ability of $Tf\text{–}I^{Tf}_{A488/A647}$ to capture spatiotemporal maps of transferrin trafficking were carried out in scFv–furin-expressing IA2.2 cells. EE/SEs were marked with $Tf\text{–}I^{Tf}_{A488/A647}$ as described. Figure 3j shows SEs distributed throughout the cytoplasm, and a frequency distribution of their pH shows an average of 6.09 ± 0.01 (Fig. 3j–l). A further 12 min chase resulted in $Tf\text{–}I^{Tf}_{A488/A647}$ labelling the pericentriolar REs (Fig. 3m), which demonstrated a substantially higher D/A corresponding to a pH of 6.35 ± 0.04 characteristic of REs (Fig. 3n,o)[19]. This indicates that each programmed DNA nanomachine (i) follows the endocytic pathway it is programmed to target, (ii) quantitatively recapitulates its pH-sensing characteristics inside cells, and (iii) provides high-resolution spatiotemporal pH maps of those subcellular organelles whose pH it was designed to report.

Simultaneous pH mapping along two endocytic pathways

We then sought to simultaneously map spatiotemporal pH changes along both endocytic pathways. We demonstrate two different methods to achieve this: (i) timed pulse/chase of cells with solutions of $Tf\text{–}I^{Tf}_{A488/A647}$ and $I^{Fu}_{A546/A647}$ sequentially, localizing them in different endocytic compartments along each pathway, and (ii) a simultaneous pulse/chase of a cocktail of $Tf\text{–}I^{Tf}_{A488/A647}$ and $I^{Fu}_{A546/A647}$, delivering both nanomachines into the same endocytic compartment from where, with time, they segregate into different organelles along each pathway.

As an example, we describe in detail how both DNA nanomachines are used sequentially to mark EE/SEs and LEs of the transferrin receptor and furin endocytic pathways, respectively (Supplementary Fig. S10). scFv–furin-expressing IA2.2 cells were first pulsed with 500 nM $I^{Fu}_{A546/A647}$ for 10 min, washed, then chased for 45 min to mark all the LEs on the furin pathway. After a chase of 45 min, the same cells were pulsed with 500 nM $Tf\text{–}I^{Tf}_{A488/A647}$ for 10 min, which marked all the EE/SEs. Figure 4a–g presents images of a typical cell marked as described above. Figure 4a,b shows the images in the donor (520 nm) and FRET (669 nm) channels when A488 on $Tf\text{–}I^{Tf}_{A488/A647}$ is excited. Figure 4c shows an overlay of the intensities in the donor (magenta) and FRET (blue) channels, giving a qualitative indication of pH heterogeneity in the EE/SEs marked with $Tf\text{–}I^{Tf}_{A488/A647}$, which is quantified in Fig. 4h. Similarly, Fig. 4d–f presents images of the same cell marked by $I^{Fu}_{A546/A647}$. Figure 4d,e shows the intensities in the donor (570 nm) and FRET (669 nm) channels when A546 on $I^{Fu}_{A546/A647}$ is excited, and Fig. 4f presents an overlay of the intensities in the donor (red) and FRET (green) channels, respectively, giving a qualitative indication of pH heterogeneity in the LEs marked with $I^{Fu}_{A546/A647}$. This is quantified in Fig. 4i. Figure 4g shows an overlay of the images of Fig. 4c and f that reveals the ability of programmed DNA nanomachines to capture the spatial pH heterogeneity of two types of endocytic compartments, namely SEs and LEs, simultaneously within the same cell. Similarly, we could obtain spatial pH maps of REs and LEs using $Tf\text{–}I^{Tf}_{A488/A647}$ and $I^{Fu}_{A546/A647}$ (Supplementary Fig. S11). Figure 4j shows a representative image for the SimpHony spatial pH map on REs and LEs that is analogous to Fig. 4g, quantified in Fig. 4k and l, respectively, the results of which are consistent with the values expected for these organelles (Supplementary Table S2). Figure 4m shows a representative SimpHony spatial pH map of the EE/SEs and TGN revealed by $Tf\text{–}I^{Tf}_{A488/A647}$ and $I^{Fu}_{A546/A647}$, respectively, and the reported pH heterogeneity is quantified in Fig. 4n,o (Supplementary Fig. S12). Figure 4p shows a representative SimpHony spatial pH map of the REs and TGN revealed by $Tf\text{–}I^{Tf}_{A488/A647}$ and $I^{Fu}_{A546/A647}$, and the reported pH heterogeneity of these organelles is quantified in Fig. 4q,r (Supplementary Fig. S13). Importantly, the pH values of each of these organelles revealed by SimpHony showed correspondence with the non-SimpHony values that used only one DNA nanomachine (Supplementary Table S2).

Having demonstrated SimpHony in organelles where both DNA nanomachines occupy two distinct compartments, we sought to explore whether both DNA nanodevices could work in tandem within the same compartment and report pH dynamics. We therefore incubated scFv–furin-expressing IA2.2 cells with a mixture of $I^{Fu}_{A546/A647}$ and $Tf\text{–}I^{Tf}_{A488/A647}$ for 10 min, followed by washing and imaging. This resulted in abundant co-localization of $I^{Fu}_{A546/A647}$ and $Tf\text{–}I^{Tf}_{A488/A647}$ in the EE/SEs (Fig. 4s–u), and the pH heterogeneity captured by each DNA nanomachine was quantified. We found

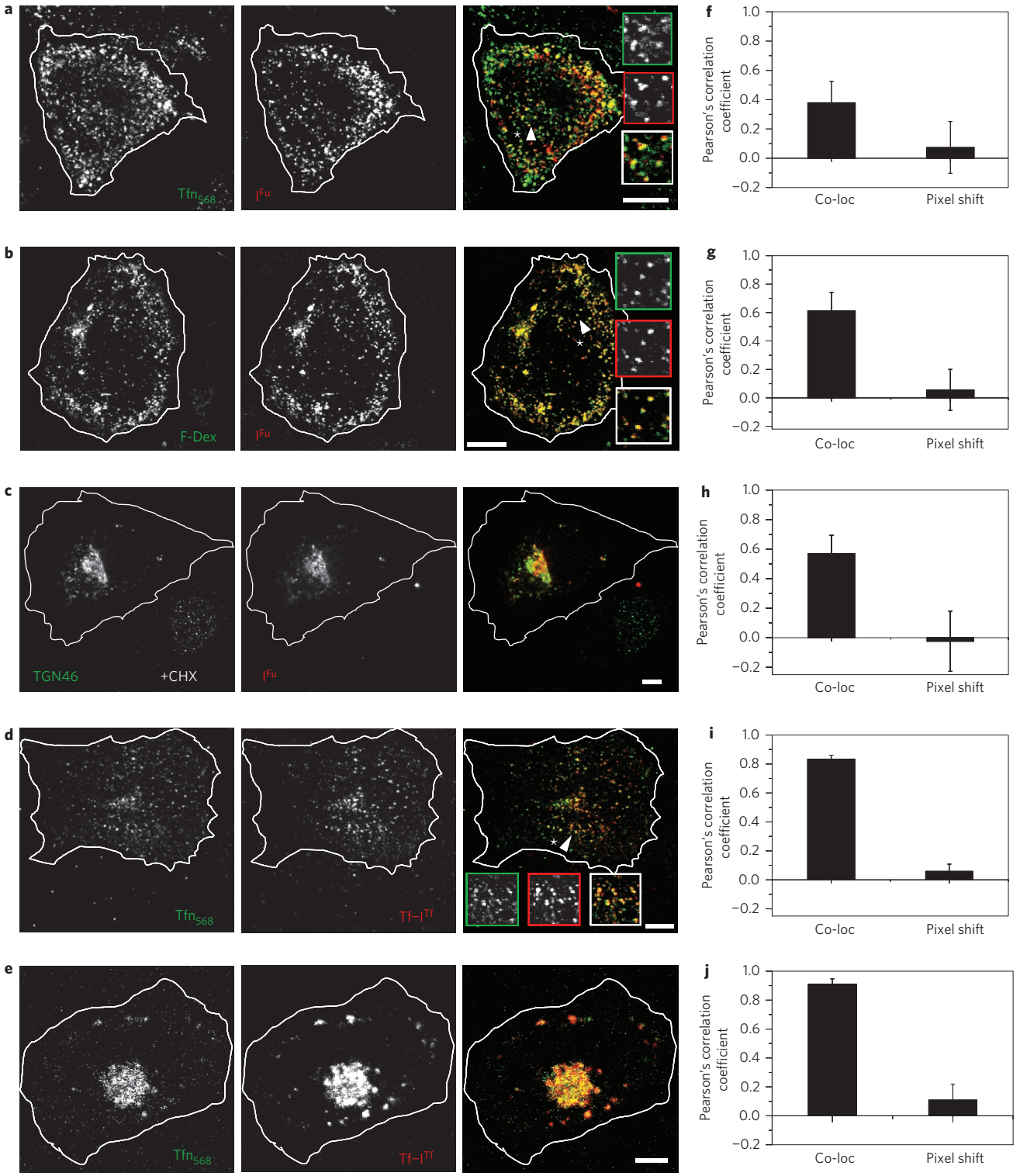

Figure 2 | Programmed trafficking of DNA nanomachines along two distinct endocytic pathways. a–c, Trafficking of I^{Fu} along the furin pathway. Representative single-plane confocal images showing co-localization of $I^{Fu}_{A488/A647}$ and EE/SE marker transferrin-A568 (Tfn_{A568}) (**a**), $I^{Fu}_{A546/A647}$ and LE marker FITC-dextran (F-Dex) (**b**) and $I^{Fu}_{A546/A647}$ and TGN marker TGN46 (**c**), in the presence of cycloheximide (CHX), stained with mouse anti TGN46. **d,e**, Tf–I^{Tf} trafficking along the transferrin receptor pathway. Cells were co-pulsed with Tf–$I^{Tf}_{A488/A647}$ and Tfn_{568} for 10 min for SE/EE labelling (**d**) or with Tf–$I^{Tf}_{A488/A647}$ and Tfn_{568} for 10 min followed by a brief chase of 12 min for RE labelling (**e**). **f–j**, Quantification of co-localization between the DNA nanomachines and endosomal markers used in **a–e**. Values indicate mean of >10 cells (**f,g,j**) and 20 cells (**h,i**) ± s.d. Cell boundaries are demarcated by white outlines. Experiments were performed in duplicate. Scale bars, 10 μm (**a–d**) and 5 μm (**e**).

that Tf–$I^{Tf}_{A488/A647}$ revealed a pH spread of 5.93 ± 0.16 (Fig. 4v), and $I^{Fu}_{A546/A647}$ a highly consistent spread of 6.0 ± 0.05 (Fig. 4w). These were also in very good agreement with EE/SE pH distributions as mapped with either DNA nanomachine alone (Fig. 4x,y, Supplementary Table S2), indicating that crosstalk between the DNA nanodevices is insignificant. This demonstrates that both

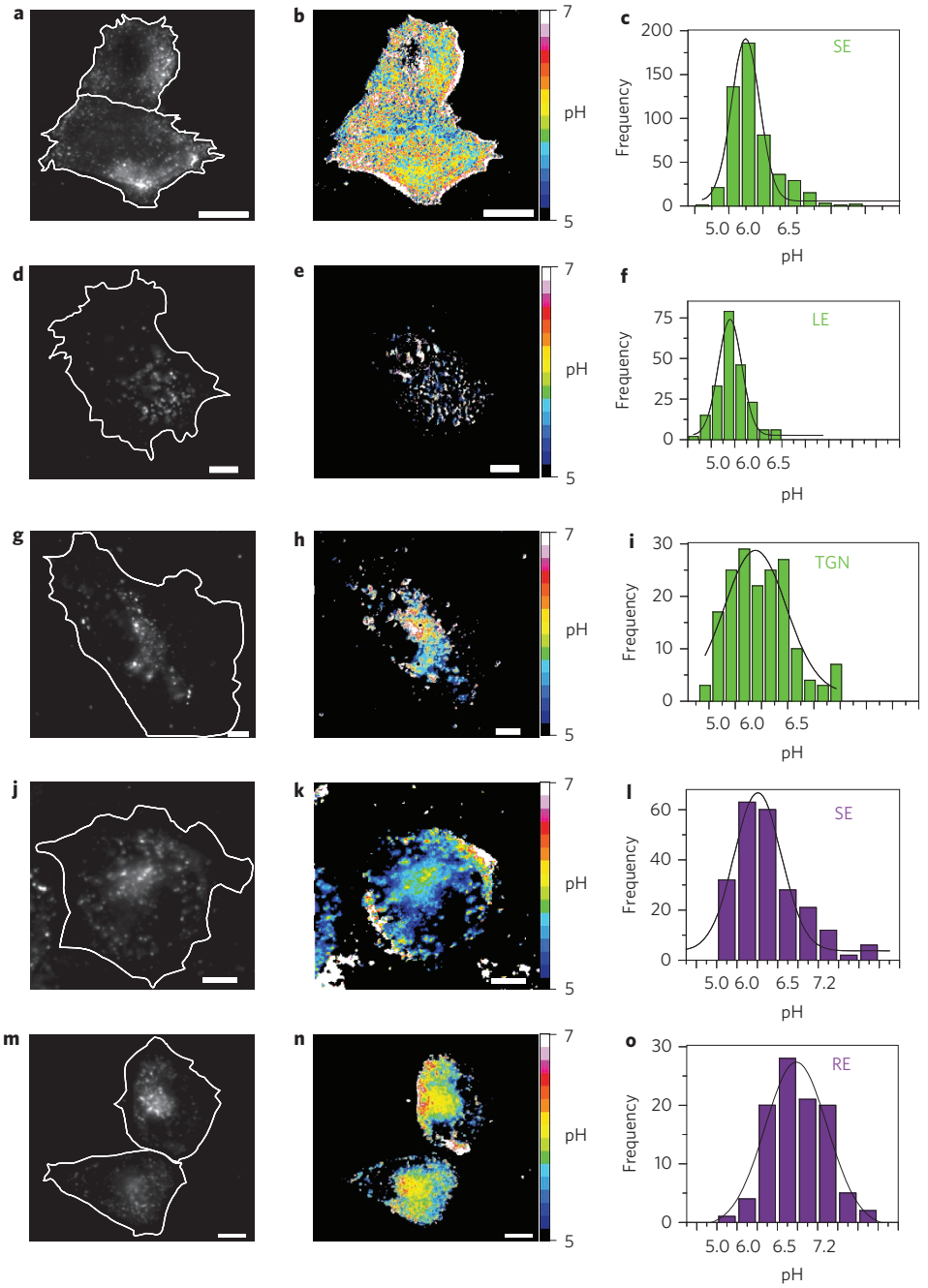

Figure 3 | *In cellulo* performance of DNA nanomachines. Temporal pH maps of endosomal organelles using Tf-$I^{Tf}_{A488/A647}$ and $I^{Fu}_{A546/A647}$. **a**,**b**,**d**,**e**,**g**,**h**, Wide-field images showing scFv-furin-expressing cells (demarcated by white outlines) pulsed at 37 °C with $I^{Fu}_{A546/A647}$ for 10 min and imaged (**a**,**b**); pulsed for 30 min, chased for 45 min and imaged (**d**,**e**); or pulsed for 2 h, chased for 90 min in CHX and imaged (**g**,**h**). **c**,**f**,**i**, pH distributions of EE/SE (**c**), LE (**f**) and TGN (**i**) as revealed by $I^{Fu}_{A546/A647}$. **j**,**k**,**m**,**n**, Cells were labelled with Tf-$I^{Tf}_{A488/A647}$ for 10 min and imaged (**j**,**k**), or labelled for 10 min, chased for 12 min and imaged (**m**,**n**). **l**,**o**, pH distribution of SE (**l**) and RE (**o**), as revealed by Tf-$I^{Tf}_{A488/A647}$. **b**,**e**,**h**,**k**,**n**, Corresponding pseudocolour D/A map of cells typically marked with Tf-I^{Tf} and I^{Fu}. Experiments were performed in duplicate. Scale bars, 10 μm.

DNA nanomachines function autonomously within the cell, independently of one another, even when present in the same compartment, reaffirming the non-interfering nature of DNA-based pH-sensitive nanodevices.

SimpHony reveals organelle morphology and pH

Given that SimpHony provides high-precision and simultaneous pH maps, we sought to apply it to capture functional pH correlates associated with known perturbations of organelle morphology. Dynamin is known to interact with actin nucleation-promoting factor WASH, which, when blocked, inhibits EE fission, causing EE tubulation and arresting endosomal dynamics[22]. Chemical inhibition of dynamin by dynasore also arrests endosomal dynamics, tubulates the EE, and prevents endosomal maturation[23]. It has been predicted that such dynasore-mediated inhibition of fission could result in hypoacidification of the EE, which affects endosomal maturation[23,24]. We applied SimpHony to this system by marking EEs with Tf-$I^{Tf}_{A488/A647}$ and LEs with $I^{Fu}_{A546/A647}$ in the presence and absence of dynasore[23]. In the absence of dynasore, EEs exhibited active dynamics and showed an average pH of 6.05 ± 0.07 (Fig. 5a,c;

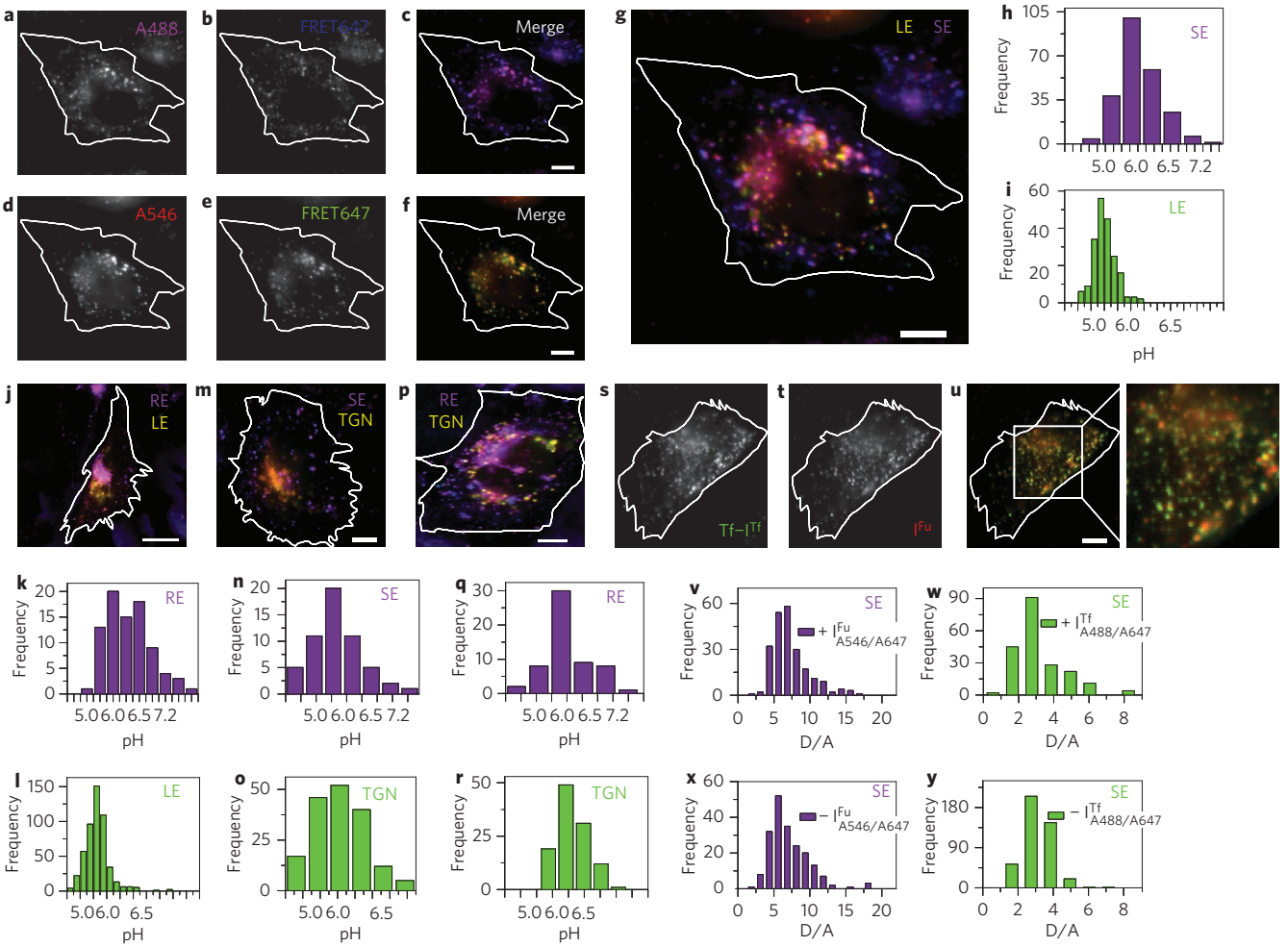

Figure 4 | SimpHony of transferrin receptor and furin endocytic pathways. a–w, Sequential (**a–r**) and simultaneous (**s–w**) pulses. SimpHony of EEs (**a–c**) and LEs (**d–f**). Simultaneous pH maps (**g**) of EEs and LEs labelled with Tf–$I^{Tf}_{A488/A647}$ and $I^{Fu}_{A546/A647}$, respectively. EE/SEs are shown in magenta and blue (A488 and FRET647 channel, respectively). LEs are shown in red and green (A546 and FRET647 channel, respectively). Quantification of pH heterogeneity of EE/SEs (**h**) and LEs (**i**). SimpHony of REs and LEs (**j–l**) marked with Tf–$I^{Tf}_{A488/A647}$ and $I^{Fu}_{A546/A647}$, respectively, and their corresponding pH distributions. SimpHony of EE/SEs and TGN (**m–o**) marked with Tf–$I^{Tf}_{A488/A647}$ and $I^{Fu}_{A546/A647}$, respectively, and their corresponding pH distributions. SimpHony of REs and TGN (**p–r**) marked with Tf–$I^{Tf}_{A488/A647}$ and $I^{Fu}_{A546/A647}$, respectively and their corresponding pH distributions. Co-localization of Tf–$I^{Tf}_{A488/A647}$ and $I^{Fu}_{A546/A647}$ in the EE (**s–u**) after a simultaneous pulse for 10 min. pH distribution of EEs revealed simultaneously by Tf–$I^{Tf}_{A488/A647}$ (**v**) and $I^{Fu}_{A546/A647}$ (**w**). **x**,**y**, pH heterogeneity of EEs revealed by Tf–$I^{Tf}_{A488/A647}$ alone (**x**) or $I^{Fu}_{A546/A647}$ alone (**y**). Cell boundaries are demarcated by white outlines. Experiments were performed in duplicate. Scale bars, 5 μm.

Supplementary Fig. S14, Movies S1, S4), while LEs showed an average pH of 5.43±0.3 (Fig. 5d). In the presence of 160 μM dynasore, we observed arrested dynamics and characteristic EE tubulation (Fig. 5b; Supplementary Fig. S14, Movies S2, S5)[22,23]. SimpHony revealed that this tubulation was also accompanied by a clear elevation of lumenal pH spanning 6.1–6.7 (mean pH 6.58±0.19) (Fig. 5e). In contrast, the lumenal pH of LEs showed negligible change (5.44±0.38) (Fig. 5f). Importantly, when dynasore was washed out, EE tubulation was abolished, endosomal dynamics was regained (Supplementary Fig. S14, Movie S3), and the average pH of the EEs was completely restored (Fig. 5g). Additionally, at all steps with and without dynasore, the lumenal pH of another related organelle (such as the LEs) remained unaffected (Fig. 5d,f,h). SimpHony revealed that in these voluminous and tubular EEs, there is indeed hypoacidification of the lumen.

Having captured the predicted defective acidification associated with a morphological change of an organelle such as the EE, we applied SimpHony to another very important alteration of organelle morphology that has been extensively studied but where functional pH correlates have so far remained elusive. The fungal metabolite brefeldin A causes extensive tubulation of the TGN, which then collapses around the microtubule organizing centre, accompanied by the rapid redistribution of Golgi resident proteins into the endoplasmic reticulum[25–27]. For example, upon treatment with brefeldin A, the TGN resident mannose-6-phospate receptor is distributed in the tubules and fuses with transferrin-containing EEs, while furin-positive tubules originating from the TGN are devoid of transferrin (Supplementary Fig. S15a,b)[28,29]. We therefore applied SimpHony to brefeldin A-induced tubules marked by $I^{Fu}_{A546/A647}$ while simultaneously marking transferrin-containing endosomes with Tf–$I^{Tf}_{A488/A647}$. Treated cells showed tubular extensions emerging from compartments localized near the microtubule organizing centre (Supplementary Fig. S15a). Tf–$I^{Tf}_{A488/A647}$ in these cells mainly occupied the excluded space of $I^{Fu}_{A546/A647}$ in the region around the microtubule organizing centre (Supplementary Fig. S16a,b). Co-localization of $I^{Fu}_{A488/A647}$ with both anti-TGN46 and NBD ceramide confirmed that the brefeldin A-induced tubules were indeed TGN related (Fig. 5i,j,

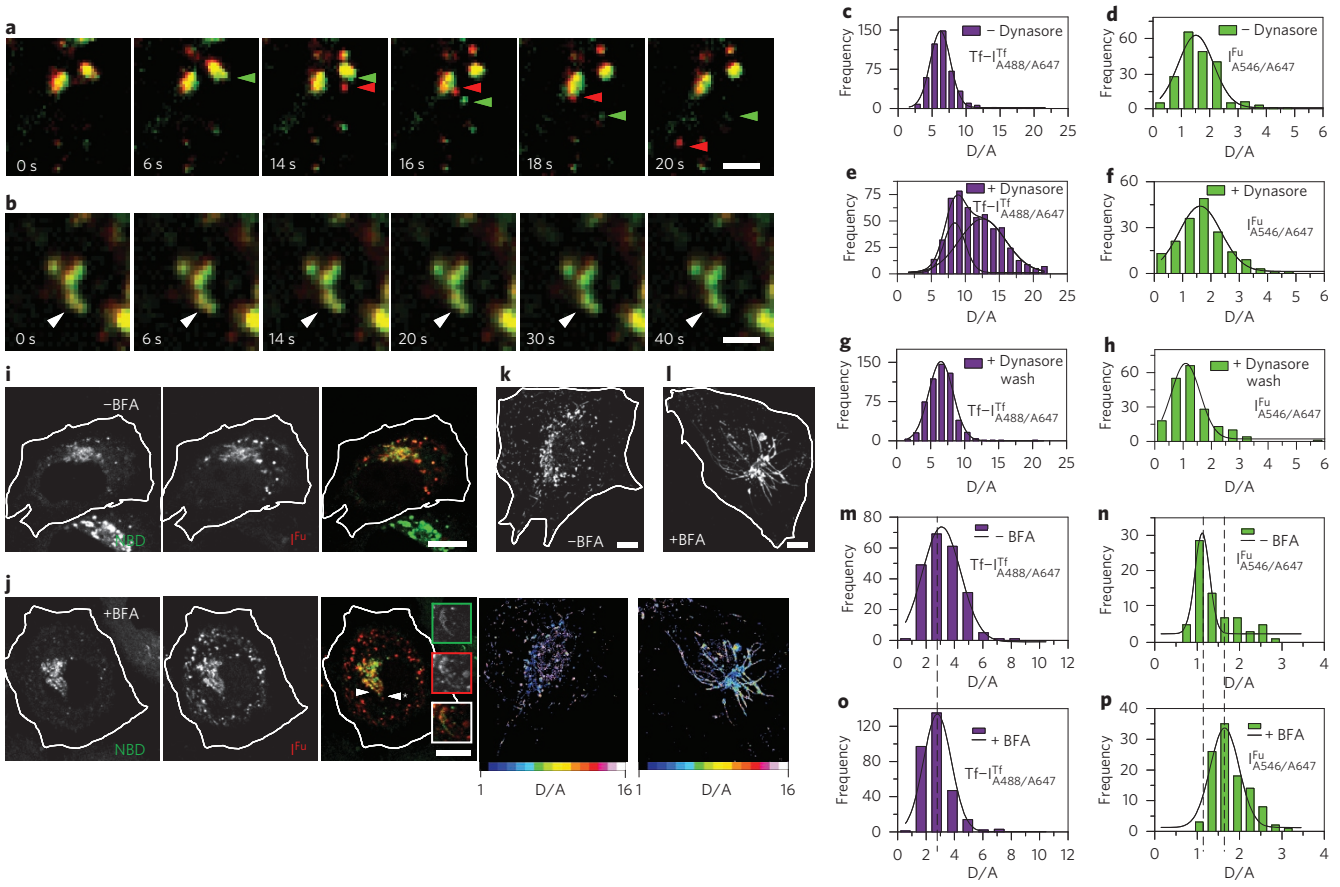

Figure 5 | SimpHony of organelles with altered morphology. a,**b**, Time-lapse images of EEs labelled with Tf–$I^{Tf}_{A488/A647}$ and $I^{Fu}_{A546/A647}$ showing active and arrested dynamics in the absence (**a**) and presence (**b**) of 160 μM dynasore, respectively. $I^{Fu}_{A546/A647}$ and Tf–$I^{Tf}_{A488/A647}$ co-localize in EEs (yellow pixels). Green and red arrowheads indicate endosomes containing Tf–I^{Tf} and I^{Fu}, respectively, segregating their individual pathways due to EE fission. In the presence of dynasore, EE fission is blocked, retaining both $I^{Fu}_{A546/A647}$ and Tf–$I^{Tf}_{A488/A647}$ in EEs (yellow pixels, shown by a white arrowhead). **c**–**h**, SimpHony of EEs and LEs revealed by Tf–I^{Tf} and I^{Fu}, respectively, in the absence (**c**,**d**), presence (**e**,**f**) and after washing out (**g**,**h**) dynasore. **i**–**p**, SimpHony of TGN in the presence of brefeldin A (BFA). TGN was labelled with $I^{Fu}_{A546/A647}$ and stained with NBD-C6-ceramide in the absence (**i**) or presence (**j**) of brefeldin A for 10 min. Inset in **j**: zoomed images (green, NBD; red, I^{Fu}; white, merged image) of regions corresponding to the right arrowhead and asterisk; the left arrowhead indicates the TGN. **k**,**l**, pH maps of TGN. Cells were marked with $I^{Fu}_{A546/A647}$, as described in the main text, and imaged in the absence (**k**) or presence (**l**) of BFA. The top panel represents the greyscale image, and the bottom panel represents its corresponding pseudocolour D/A image. Pixels are colour coded on the basis of their D/A ratios, with blue pixels denoting low D/A ratios and red pixels indicating high D/A ratios. In **i**–**l**, all images are single-plane confocal images, with individual cells demarcated by a white outline. **m**–**p**, SimpHony of EE and TGN revealed by Tf–I^{Tf} and I^{Fu}, respectively: pH distribution of EEs (**m**,**o**); pH distribution of the TGN (**n**,**p**). Experiments were performed in triplicate. Scale bars, 3 μm (**a**,**b**) and 10 μm (**i**–**l**).

Supplementary Fig. S17). pH heat maps of treated and untreated cells showed striking pH differences in $I^{Fu}_{A546/A647}$-containing compartments, where brefeldin A-induced tubules showed markedly high D/A values and a strikingly elevated pH of 6.35±0.17 (Fig. 5k,l). In contrast, D/A values of EEs marked by Tf–$I^{Tf}_{A488/A647}$ demonstrated negligible pH change (Fig. 5m,o, Supplementary Figs S18, S19, Table S3). Untreated cells revealed a mean EE/SE pH of 6.07±0.07 and a lumenal TGN pH of 5.94±0.15 (Fig. 5n,p, Supplementary Fig. S19, Table S3). Thus SimpHony reveals that the tubulation of the TGN substantially lowers its lumenal acidity. SimpHony therefore demonstrates that significant perturbation of a physical characteristic such as the morphology of a subcellular compartment results in defective acidification, which could be linked to the observed impairment of protein trafficking through such compartments.

Conclusions

We have exploited the programmable nature of DNA scaffolds to precisely position DNA nanodevices in distinct intracellular compartments by tagging them to specific trafficking proteins. The modular nature of DNA allows the integration of analyte-sensing domains with protein recognition domains without perturbing the recognition properties of either domain. The synthetic nature of designer DNA scaffolds allows the incorporation of organic fluorophores, allowing the tracking of protein localizations while simultaneously reporting their ionic environments using a two-colour readout. We have taken advantage of the molecularly programmable nature of DNA scaffolds to access functionality inaccessible to any other molecular scaffold—the ability to sense the same analyte, simultaneously, in distinct intracellular locations—by using two different DNA nanomachines each programmed to tack onto a different protein within the same cell.

It should be noted that the pH-sensitive DNA nanodevices described here have narrower ranges than the corresponding small-molecule sensors and can therefore provide pH maps with much greater resolution than small-molecule sensors. Given the engineerability of the DNA scaffold and the fact that i-motif stability is tunable, a range of pH sensors suited to different pH regimes may be envisaged. However, a prior estimate of the anticipated pH

regime would be required before the deployment of various I-switches *in cellulo*. Furthermore, before obtaining the functional correlates offered by SimpHony for receptor trafficking pathways, it is essential to first characterize the pathways of interest using conventional methods. However, SimpHony might also provide useful clues regarding the compartment environment in cases that are less straightforward to identify.

SimpHony is applicable to a variety of compartment mixing problems, and also cellular fusion/fission problems in biology. Importantly, measures of *in vivo*/intracellular chemistry using this targeting technology are generalizable to the chemical diversity that can already be sensed by DNA to access functionally richer chemical maps of cells. Organelle targeting and simultaneous chemical mapping technology using DNA nanodevices thus offers substantial potential for the integration of small-molecule triggers originating from subcellular environments within biological networks.

Methods

Materials. All the unlabelled oligonucleotides used were obtained from Eurofins Genomics, and labelled oligonucleotides (high-performance liquid chromatography-purified and lyophilized) were obtained from IBA, GmbH. I^{n} and $I^{n'}$ (5 μM) were mixed in equimolar ratios in 20 mM potassium phosphate buffer of the desired pH containing 100 mM KCl. The resultant solution was heated to 90 °C for 5 min, cooled to room temperature at 5 °C/15 min and equilibrated at 4 °C overnight. Solutions of I-switch at different pH values were made by diluting 1 μl of 5 μM stock samples into 99 μl of 1× clamping buffer of the desired pH. All samples were vortexed and equilibrated for 30 min at room temperature. The experiments were performed in a wide-field microscope (Nikon Eclipse Ti-U). An *in vitro* pH calibration curve was obtained by plotting the ratio of the donor intensity (D) at 520 nm and the acceptor intensity (A) at 669 nm (for A488/A647), and for 570 nm and 670 nm, respectively, for the A546/A647 pair, as a function of pH.

Determination of binding constants. The affinity and specificity of the scFv were analysed by enzyme-linked immunosorbent assay after purifying the scFv. A streptavidin-coated 96-well plate was incubated with dsDNA epitope for screening, in 5× SSCT (75 mM sodium citrate, 750 mM NaCl, 0.05% Tween-20), for 1.5 h, to immobilize the dsDNA onto the streptavidin-coated 96-well plate. For competition experiments, dsDNA immobilized onto the streptavidin-coated 96-well plate was incubated with a mixture of competing nucleic acid, purified scFv (200–300 nM) and anti myc-tag antibody (1 in 1,000 dilution) for 1.5 h at room temperature. The wells were then washed in a 1 litre PBST (1× PBS, 0.1% Tween-20) bath before the addition of the secondary antibody conjugated to horseradish peroxidase. Bound scFvs were detected by the addition of 3,3′,5,5′-tetramethyl benzidine/H_2O_2, and the optical density (OD) at 450 nm was recorded and normalized with respect to the well with no added competitor.

Cell culture and labelling with endocytic markers. HeLa cells were cultured in Dulbecco's modified eagle's medium/F-12 (1:1) (Invitrogen) containing 10% heat-inactivated fetal bovine serum (FBS) (Invitrogen), 100 μg ml^{-1} streptomycin and 100 U ml^{-1} penicillin (Invitrogen). The IA2.2 cell line is a Chinese hamster ovary (CHO) cell line that lacks endogenous transferrin receptors but stably expresses the human transferrin and folate receptors. These cells were cultured in Ham's-F12 Complete media (HF-12, Himedia) containing 10% heat-inactivated FBS, 100 μg ml^{-1} streptomycin and 100 U ml^{-1} penicillin with 200 μg ml^{-1} G418 and 100 μg ml^{-1} hygromycin to ensure maintenance of the transferrin and folate receptors. For transient transfections, cells were plated at >50% density onto a coverslip-bottomed 35 mm dish and 150 ng of scFv–furin construct was introduced using the Lipofectamine 2,000 reagent system (Invitrogen), following the manufacturer's instructions. Cells were imaged 24 h after transfection. For I-switch labelling, $I^{Fu}_{A488/A647}$ was diluted in labelling media to a final concentration of 500 nM, and Tf-conjugated switch (Tf–$I^{Tf}_{A488/A647}$) was diluted in M1 and incubated for different times at 37 °C. For labelling LEs, cells were incubated with $I^{Fu}_{A488/A647}$ and 2 mg ml^{-1} FITC dextran in labelling media at 37 °C for 1 h followed by a chase for 1 h. SEs were labelled by 100 μg ml^{-1} Alexa 568-labelled human holo-transferrin after incubating IA2.2 cells at 37 °C for 10 min in M1, while a brief chase of 12 min marked REs. Wide-field and confocal images were collected using a Nikon inverted microscope and an Olympus Fluoview 1,000 confocal microscope, respectively. Donor and acceptor images were overlaid and endosomes showing co-localization were further quantified using ImageJ ver. 1.46.

Received 13 November 2012; accepted 22 April 2013; published online 26 May 2013

References

1. Seeman, N. C. DNA in a material world. *Nature* **421,** 427–431 (2003).
2. Bath, J. & Turberfield, A. J. DNA nanomachines. *Nature Nanotech.* **2,** 275–284 (2007).
3. Krishnan, Y. & Bathe, M. Designer nucleic acids to probe and program the cell. *Trends Cell Biol.* **22,** 624–633 (2012).
4. McMahon, D. Chemical messengers in development: a hypothesis. *Science* **185,** 1012–1021 (1974).
5. Modi, S. *et. al.* A DNA nanomachine that maps spatial and temporal pH changes inside living cells. *Nature Nanotech.* **4,** 325–330 (2009).
6. Surana, S., Bhat, J. M., Koushika, S. P. & Krishnan, Y. An autonomous DNA nanomachine maps spatiotemporal pH changes in a multicellular living organism. *Nature Commun.* **2,** 340 (2011).
7. Douglas, S. M., Bachelet, I. & Church, G. M. A logic-gated nanorobot for targeted transport of molecular payloads. *Science* **335,** 831–834 (2012).
8. Lee, H. *et al.* Molecularly self-assembled nucleic acid nanoparticles for targeted *in vivo* siRNA delivery. *Nature Nanotech.* **7,** 389–393 (2012).
9. Bhatia, D., Surana, S., Chakraborty, S., Koushika, S. P. & Krishnan, Y. A synthetic icosahedral DNA-based host–cargo complex for functional *in vivo* imaging. *Nature Commun.* **2,** 339 (2011).
10. Mallet, W. G. & Maxfield, F. R. Chimeric forms of furin and TGN38 are transported with the plasma membrane in the trans-Golgi network via distinct endosomal pathways. *J. Cell Biol.* **146,** 345–359 (1999).
11. Chia, P. Z. C., Gasnereau, I., Lieu, Z. Z. & Gleeson, P. A. Rab9-dependent retrograde transport and endosomal sorting of the endopeptidase furin. *J. Cell Sci.* **124,** 2401–2413 (2011).
12. Presley, J. F. *et al.* The End2 mutation in CHO cells slows the exit of transferrin receptors from the recycling compartment but bulk membrane recycling is unaffected. *J. Cell Biol.* **122,** 1231–1241 (1993).
13. McCafferty, J., Griffiths, A. D., Winter, G. & Chiswell, D. J. Phage antibodies: filamentous phage displaying antibody variable domains. *Nature* **348,** 552–554 (1990).
14. Geisow, M. J., D'Arcy Hart, P. & Young, M. R. Temporal changes of lysosome and phagosome pH during phagolysosome formation in macrophages: studies by fluorescence spectroscopy. *J. Cell Biol.* **89,** 645–652 (1981).
15. Llopis, J., McCaffery, J. M., Miyawaki, A., Farquhar, M. G. & Tsien, R. Y. Measurement of cytosolic, mitochondrial, and golgi pH in single living cells with green fluorescent proteins. *Proc. Natl Acad. Sci. USA* **95,** 6803–6808 (1998).
16. Kim, J. H. *et al.* Noninvasive measurement of the pH of the endoplasmic reticulum at rest and during calcium release. *Proc. Natl Acad. Sci. USA* **95,** 2997–3002 (1998).
17. Molloy, S. S., Thomas, L., VanSlyke, J. K., Stenberg, P. E. & Thomas, G. Intracellular trafficking and activation of the furin proprotein convertase: localization to the TGN and recycling from the cell surface. *EMBO J.* **13,** 18–33 (1994).
18. Molloy, S. S., Anderson, E. D., Jean, F. & Thomas, G. Bi-cycling the furin pathway: from TGN localization to pathogen activation and embryogenesis. *Trends Cell Biol.* **9,** 28–35 (1999).
19. Presley, J. F., Mayor, S., McGraw, T. E., Dunn, K. W. & Maxfield, F. R. Bafilomycin A1 treatment retards transferrin receptor recycling more than bulk membrane recycling. *J. Biol. Chem.* **272,** 13929–13936 (1997).
20. Yamashiro, D. J. & Maxfield, F. R. Acidification of morphologically distinct endosomes in mutant and wild-type Chinese hamster ovary cells. *J. Cell Biol.* **105,** 2723–2733 (1987).
21. Maeda, Y., Ide, T., Koike, M., Uchiyama, Y. & Kinoshita, T. GPHR is a novel anion channel critical for acidification and functions of the Golgi apparatus. *Nature Cell Biol.* **10,** 1135–1145 (2008).
22. Derivery, E. *et al.* The Arp2/3 Activator WASH controls the fission of endosomes through a large multiprotein complex. *Dev. Cell* **17,** 712–723 (2009).
23. Mesaki, K., Tanabe, K., Obayashi, M., Oe, N. & Takei, K. Fission of tubular endosomes triggers endosomal acidification and movement. *PLoS ONE* **6,** e19764 (2011).
24. Macia, E. *et al.* Dynasore, a cell-permeable inhibitor of dynamin. *Dev. Cell* **10,** 839–850 (2006).
25. Reaves, B. & Banting, G. Perturbation of the morphology of the trans-Golgi network following Brefeldin A treatment: redistribution of a TGN-specific integral membrane protein, TGN38. *J. Cell Biol.* **116,** 85–94 (1992).
26. Sciaky, N. *et al.* Golgi tubule traffic and the effects of brefeldin A visualized in living cells. *J. Cell Biol.* **139,** 1137–1155 (1997).
27. Strous, G. J. *et al.* Brefeldin A induces a microtubule-dependent fusion of galactosyltransferase-containing vesicles with the rough endoplasmic reticulum. *Biol. Cell* **71,** 25–31 (1991).

28. Waguri, S. *et al.* Visualization of TGN to endosome trafficking through fluorescently labeled MPR and AP-1 in living cells. *Mol. Biol. Cell* **14,** 142–155 (2003).
29. Maeda, Y., Beznoussenko, G. V., Van Lint, J., Mironov, A. A. & Malhotra, V. Recruitment of protein kinase D to the trans-Golgi network via the first cysteine-rich domain. *EMBO J.* **20,** 5982–5990 (2001).

Acknowledgements

The authors thank S. Mayor, D. Lilley, A. Sarin, G.V. Shivashankar and W. Shih for critical input, and the Central Imaging and Flow Facility at NCBS for imaging. The authors also thank S. Mayor for scFv libraries and the IA2.2 cell line, and J. Bonifacino and M. Marks for the Tac-furin chimera plasmids. S.M., S.S. and S.H. thank the CSIR for research fellowships. C.N. thanks NCBS for generous support of this collaboration. Y.K. thanks the Wellcome Trust–DBT India Alliance and the Innovative Young Biotechnologist Award for funding.

Author contributions

S.M. and Y.K. conceived and designed the experiments. C.N. contributed phage display expertise. S.M. performed the *in vitro* and *in cellulo* experiments. S.S. optimized the I^{Fu} used herein, and S.H. addressed scFv–furin stability. S.M. and Y.K. analysed the data. S.M., S.S. and Y.K. co-wrote the paper and all authors commented on the manuscript.

Additional information

Supplementary information is available in the online version of the paper. Reprints and permissions information is available online at www.nature.com/reprints. Correspondence and requests for materials should be addressed to Y.K.

Competing financial interests

The authors declare no competing financial interests.